Hybrid Linear/Quadratic Time-Frequency Attributes

Richard G. Baraniuk[†], Mark Coates[†] and Philippe Steeghs[*]

[†] Department of Electrical and Computer Engineering, Rice University
6100 South Main Street, Houston, TX 77005–1892
Email: {richb, mcoates}@ece.rice.edu, Web: www.dsp.rice.edu
Fax: 713.348.6196, Tel.: 713.348.2359

[*] TNO Physics and Electronics Laboratory
P.O. Box 96864, 2509 JG The Hague, The Netherlands
Email: steeghs@fel.tno.nl
Tel.: +31 70.374.0435

EDICS Number: 2-TIFR

To appear in IEEE Trans. on Signal Processing 2001

Abstract

We present an efficient method for robustly calculating time-frequency attributes of a signal, including instantaneous mean frequency, bandwidth, kurtosis, and other moments. Most current attribute estimation techniques involve a costly intermediate step of computing a (highly oversampled) 2-d quadratic time-frequency representation (TFR), which is then collapsed to the 1-d attribute. Using the principles of hybrid linear/quadratic time-frequency analysis (time-frequency distribution series), we propose computing attributes as nonlinear combinations of the (slightly oversampled) linear Gabor coefficients of the signal. The method is both computationally efficient and accurate; it performs as well as the best techniques based on adaptive TFRs. To illustrate, we calculate an attribute of a seismic cross-section.

Keywords

time-frequency analysis, instantaneous frequency, Gabor transform, seismic signal analysis

† This work was supported by NSF grants MIP–9457438 and CCR–9973188, ONR grant N00014–99–1–0813, DARPA/AFOSR grant F49620–97–1–0513, Texas Instruments, and the Rice Consortium on Computational Seismic Interpretation.

I. INTRODUCTION

Time-frequency signal attributes have provided insights in a number of fields, from seismic analysis to neurophysiology [1], [2], [3]. Attributes applied to date include instantaneous frequency, bandwidth and kurtosis (normalised fourth-order instantaneous frequency moment) [4]. The instantaneous frequency (IF) of a real mono-component signal is defined as the rate of change of the phase of the corresponding analytic signal at a given time. This is equivalent to the first moment in frequency of the Wigner distribution of the signal normalised by its instantaneous energy. Unfortunately, when we estimate the IF either directly from the phase of the analytic signal or from the Wigner distribution, we generate estimates with high variance, particularly in noisy environments [5]. Estimates based on the first moment in frequency of other time-frequency representations (TFRs) — the spectrogram, for instance — reduce the variance at the expense of some bias.

The peak of the Wigner distribution or another suitable TFR offers another attractive alternative for IF estimation. The variance of an estimate based on TFR peaks is reduced compared to moment-based methods, especially in low SNR environments. In particular, iterative methods involving repeated calculation of TFRs have proven extremely effective [5], [6], [7].

There are instances, however, when peak-based estimates are unsatisfactory. When multiple components are present in a signal, it is more desirable to calculate the moment-based IF estimate. Such is the case in the seismic analysis presented in Figure 1 and Section V. We then need a high resolution, signal-adaptive TFR to make the IF estimate useful. Unfortunately, generating such TFRs is computationally wasteful, since we merely collapse the 2-d TFR to a 1-d attribute.

[Figure 1 about here.]

In this paper, we present a computationally efficient method for estimating moment-based time-frequency attributes that avoids the calculation of a quadratic TFR altogether. Our approach exploits the *time-frequency distribution series* concept developed by Qian, Morris, and Chen [8], [9], [10] and requires only a sparse linear signal decomposition. We will present a general procedure for calculating a range of attributes but focus on IF and instantaneous bandwidth estimation for concreteness.

Section II reviews time-frequency distribution series, and Section III examines IF and its estimation. Section IV presents the new estimation technique for IF and instantaneous bandwidth, and Section V discusses its application to seismic data analysis. We make some concluding remarks in Section VI.

II. Hybrid Time-Frequency Representations

Qian, Morris, and Chen [8], [9] proposed a method for time-frequency analysis that utilises both a linear TFR (the Gabor transform) and a quadratic TFR (the Wigner distribution) to generate a signal adaptive nonlinear TFR. The Gabor transform decomposes a signal $x(t)$ in terms of logons [11] or time-frequency atoms:

$$\begin{aligned} x(t) &= \sum_{(m,n)} c_{m,n}\phi_{m,n}(t), \quad (m,n) \in \mathbb{Z}^2, & (1) \\ c_{m,n} &:= \left\langle x, \widetilde{\phi}_{m,n} \right\rangle := \int_{-\infty}^{\infty} x(t)\, \widetilde{\phi}^{*}_{m,n}(t)\, dt\,. & (2) \end{aligned}$$

The synthesis atoms are generated by time-frequency shifting a prototype atom $g(t)$ by discrete step sizes T and F:

$$\phi_{m,n}(t) := e^{j2\pi mFt} g(t - nT). \tag{3}$$

The $\widetilde{\phi}$ are dual atoms derived from ϕ [8], [11]. A natural choice for the prototype atom g is the Gaussian, since it has optimal concentration and localisation in time-frequency and a strictly positive Wigner distribution [12]. In order for (1) to be a stable representation with Gaussian atoms requires a mild oversampling in the time-frequency plane.

The auto-Wigner distibution (WD) of a signal $x(t)$ is defined as:

$$W_x(t,f) := \int_{-\infty}^{\infty} x\left(t + \tau/2\right) x^*\left(t - \tau/2\right) e^{-j2\pi f\tau}\, d\tau. \tag{4}$$

The cross-Wigner distribution between two signals $x(t)$ and $y(t)$ is defined as:

$$W_{xy}(t,f) := \int_{-\infty}^{\infty} x\left(t + \tau/2\right) y^*\left(t - \tau/2\right) e^{-j2\pi f\tau}\, d\tau. \tag{5}$$

Inserting (1) in (4) and using (5), the auto-Wigner distribution can be decomposed as:

$$\begin{aligned} W_x(t,f) &= \sum_{(m,n)} \left|c_{m,n}\right|^2 W_{\phi_{m,n}}(t,f) \\ &+ \sum_{(m,n)\neq(m',n')} c_{m,n} c^{*}_{m',n'} W_{\phi_{m,n},\phi_{m',n'}}(t,f)\,. \end{aligned} \tag{6}$$

This expression identifies two distinct contributions to the WD. The first summation in (6) corresponds to a linear sum of the (strictly positive) auto-WDs of the time-frequency atoms; it provides an approximate description of the signal's time-frequency behaviour without capturing many details. The second summation involves all of the cross-WDs between different atoms in the Gabor decomposition. The cross-WDs in this summation may be positive or negative.

The key observation is this [8], [9]: the cross-WDs between closely spaced ((m,n) close to (m',n')) atoms generally refine the time-frequency representation of the signal, whereas the cross-WDs between distant ((m,n) far from (m',n')) atoms generate global interference terms that hamper interpretation.

Qian, Morris, and Chen generate a time-frequency distribution series — which we term a *hybrid TFR* [10]) — by retaining all of the auto-WD terms in the first summation of (6), but only those cross-WDs arising from closely spaced atoms. Due to the elliptical or circular symmetry of the Gaussian atom, the Euclidean distance metric is the most natural measure of atom separation; the l_1 metric (Manhattan distance) $d\left[(m,n),(m',n')\right] := |m-m'|+|n-n'|$ is a good approximation with a lower computational complexity. Given a threshold distance δ, second summation terms are included in the final representation only if the distance between the interacting atoms is less than δ. The hybrid method thus produces a δ-parameterised class of TFRs:

$$\begin{aligned} \widetilde{W_x}^{(\delta)}(t,f) \;&:=\; \sum_{(m,n)} |c_{m,n}|^2\, W_{\phi_{m,n}}(t,f) \\ &+ \sum_{0<d[(m,n),(m',n')]<\delta} c_{m,n}c^*_{m',n'} W_{\phi_{m,n},\phi_{m',n'}}(t,f)\,. \end{aligned} \tag{7}$$

The parameter δ controls the trade-off between component resolution and interference. By a suitable selection of δ, high resolution TFRs are generated; moreover they can be determined at a much lower computational expense than signal-adaptive quadratic TFRs [13] offering similar performance. The auto- and cross-WDs in (7) are signal-independent and hence can be analytically computed and stored in memory. The computational demands of the Gabor transform are also much less than those of quadratic TFRs. By replacing the Gabor decomposition with a wavelet transform, we can generate high-resolution, low-interference time-scale representations [10].

III. INSTANTANEOUS FREQUENCY AND INSTANTANEOUS BANDWIDTH

The instantaneous amplitude $a(t)$ and IF $v(t)$ of a real-valued signal $x(t)$ are defined in terms of the analytic signal $z_x(t)$ [12], [14], [15] as:

$$\begin{aligned} a(t) &:= |z_x(t)| \\ v(t) &:= \frac{1}{2\pi}\frac{d}{dt}\arg z_x(t)\,. \end{aligned} \tag{8}$$

For signals observed in noise, one means of estimating the IF of a discrete signal is immediately clear. We can apply (8) directly to the observed signal; we call this the *complex-trace IF estimate.* Unfortunately, such an estimate is extremely susceptible to noise.

More robust estimates can be formed by considering the relationship between the WD and the IF [12], [15]:

$$v(t) = \frac{\int_{-\infty}^{\infty} f\, W_x(t,f)\, df}{\int_{-\infty}^{\infty} W_x(t,f)\, df}\,. \tag{9}$$

Direct utilisation of this formula again leads to high-variance estimates in noisy environments. However, bias can be traded against variance by replacing the Wigner distribution with a smoother TFR — the spectrogram, for instance. To obtain a good trade-off and robustly track the IFs of signals whose time-frequency behaviour is unknown and variable, we generally have to calculate a computationally intensive adaptive TFR [13]. Whichever TFR is chosen, considerable computational effort is wasted, since we generate a highly-redundant description of the 2-d, time-frequency nature of the signal merely to collapse back to the 1-d quantity $v(t)$.

The bandwidth of a signal at a particular moment in time (instantaneous bandwidth [14]) is closely related to the second-order frequency moment of a TFR P_x of the signal:

$$B_P^2(t) = \frac{\int_{-\infty}^{\infty} f^2 P_x(t,f)\, df}{\int_{-\infty}^{\infty} P_x(t,f)\, df} - v(t)^2. \tag{10}$$

As the resolution of the TFR improves, its second-order moment provides a better indication of instantaneous bandwidth. However, interference terms and noise make bandwidth estimates based on the high-resolution WD unstable.

IV. HYBRID INSTANTANEOUS FREQUENCY AND BANDWIDTH CALCULATION

In this section, we detail how the hybrid TFR approach of Section II can be adopted to robustly estimate the IF and instantaneous bandwidth. Our approach requires the much smaller computational expense of determining a linear, mildly over-sampled Gabor representation of the signal.

Substituting the Gabor expansion of the signal (1), we can rewrite the numerator of (9) as

$$\sum_{(m,n,m',n')} c_{m,n} c^*_{m',n'} \int_{-\infty}^{\infty} f\, W_{\phi_{m,n}}(t,f)\, df\,. \tag{11}$$

When we use a Gaussian of variance σ^2 for the Gabor synthesis atom, closed-form expressions can be developed for the integrals in the summation.[1] Applying the same expansion to the denominator, we can express (9) as

$$v(t) = \frac{\sum_{m,n,m',n'} c_{m,n} c^*_{m',n'} V_{m,n,m',n'}(t)}{\sum_{m,n,m',n'} c_{m,n} c^*_{m',n'} A_{m,n,m',n'}(t)} \tag{12}$$

where

$$A_{m,n,m',n'}(t) := \frac{1}{2\pi} \exp\left[-j2\pi(n-n')Ft\right] \times \exp\left[-\frac{(t-mT)^2 + (t-m'T)^2}{2\sigma^2}\right] \tag{13}$$

and

$$V_{m,n,m',n'}(t) := \left[\frac{-j(m-m')T}{4\pi\sigma^2} - \frac{(n+n')\,F}{2}\right] A_{m,n,m',n'}(t)\,. \tag{14}$$

If all (m,n,m',n') combinations are included in the estimate, then this formula is equivalent to the (high-variance) WD-based estimate. By adopting the hybrid TFR approach (retaining only a subset of the terms when $(m,n) \neq (m',n')$), we can reduce the variance with the introduction of some bias. The performance is of a level similar to that obtained with adaptive quadratic TFRs; however, the computational expense is much reduced, since the $A_{m,n,m',n'}(t)$ and $V_{m,n,m',n'}(t)$ are signal-independent and can be precomputed and stored in memory. The primary cost of the algorithm is then that of computing the (barely oversampled) Gabor transform.

The second-order moment of the hybrid TFR provides a similarly computationally efficient estimate of the instantaneous bandwidth:

$$B^2(t) = \frac{\sum_{m,n,m',n'} c_{m,n} c^*_{m',n'} D_{m,n,m',n'}(t)}{\sum_{m,n,m',n'} c_{m,n} c^*_{m',n'} A_{m,n,m',n'}(t)} - v^2(t) \tag{15}$$

with

$$\begin{aligned} D_{m,n,m',n'}(t) \quad &:= \quad \frac{1}{(4\pi)^2} \exp\left[-\frac{(t-mT)^2 + (t-m'T)^2}{2\sigma^2}\right] \exp\left[-j2\pi(n-n')Ft\right] \\ &\quad \times \left[-\frac{(T(m-m'))^2}{\sigma^4} + \frac{2 + 4\pi jTF(m-m')\,(n+n')}{\sigma^2} + 4\pi^2\left(F(n+n')\right)^2\right]. \end{aligned} \tag{16}$$

---

[1] Similar analytic expressions are possible for other windows, including, for example, square, triangle, and raised cosine windows.

Figure 2 shows a comparison between the instantaneous bandwidth measures computed using the spectrogram and the hybrid TFR approach. One hundred random bandpass signals were generated by applying a time-varying filter to white Gaussian noise realisations. Figure 2(a) depicts the ideal frequency response of the filter. Figure 2(b) plots two lines for each technique; the lines show the averages of $v(t) \pm B(t)$ over the one hundred realisations. Clearly the hybrid TFR bandwidth estimate tracks the true bandwidth characteristics of the signal far more closely than the spectrogram-based measure.

[Figure 2 about here.]

If the hybrid estimate if formed without cross-terms, then the performance is very similar to the spectrogram. We can provide no strict guidelines regarding the choice of the distance threshold. In our experiments, we have observed that Manhattan distance thresholds δ between 1 and 3 provide good results. Setting $\delta = 1$ results in more smoothing and hence more robust estimates in very noisy environments. The choice of $\delta = 3$ reduces the bias of estimates and is appropriate when there is little noise and a single dominant signal component.

It is possible to extend our method to estimate signal attributes derived from higher-order moments. In particular, we can estimate instantaneous skew and instantaneous kurtosis [4] in a similar fashion, but the third- and fourth-order terms generate more complicated expressions that we do not provide here.

V. Application to Seismic Data Analysis

As an example of the hybrid IF estimation procedure, we now consider an application in seismic data analysis. Seismic imagery of the earth's subsurface is critical to all aspects of the oil and gas exploration process — from the location of reserves to their appraisal and subsequent monitoring. A seismic image of the earth is obtained by probing the subsurface with acoustic waves. An example of a seismic cross-section is shown in Figure 3(a). The horizontal axis gives the spatial location at the surface, and the vertical axis is time. Each column of the image represents a recording of the pressure as a function of time at the corresponding surface location. The line plot to the left of the intensity image is the amplitude of the first column (like Figure 1(a)). When seismic waves propagate through the subsurface, a part of their energy is reflected back to the surface at acoustic impedance contrasts. The strength of this impedance contrast is called the *reflectivity*. The seismic cross-section represents this (bandlimited) reflectivity of the subsurface.

[Figure 3 about here.]

A change in acoustic impedance indicates a change in rock properties. As a result, it is possible to make an educated guess of the geological structure of the subsurface on the basis of the reflectivity image. If the seismic wave velocity is known, then the vertical time axis can be converted to depth. In the cross-section of Figure 3(a), a 1s two-way travel time of the seismic waves corresponds to a depth of approximately 1km. The reflectivity image is obtained from the raw data through a great number of data processing steps. The most important of these are source deconvolution, noise suppression, velocity correction, and a final imaging step (migration) [16].

In seismic exploration, seismic cross-sections are scrutinized by interpreters who search for features that indicate hydrocarbon reservoirs. While previously intepreters dealt with large plots of 2-d cross-sections, they now work on computers with 3-d volumes comprising many gigabytes of data. Currently, there is a great need for methods that can aid in rapidly sifting out those features that are relevant for the geological interpretation of the data.

Seismic attributes aid the interpretation of seismic data by elucidating its salient signal characteristics. Traditionally, complex-trace analysis via Hilbert transform (using (8)) has been used for attribute extraction [17]. The standard seismic attributes are instantaneous amplitude, phase, and frequency. The goal of *seismo-stratigraphic interpretation* is to infer the sequence of geological events that resulted in the reflection pattern observed in a seismic image [18]. In the ideal case, the seismic expression of a rock formation can be directly related to the circumstances under which the rock was formed. A seismic reflection pattern with a distinct set of image characteristics is called a *seismic facies unit*. For instance, rapid sedimentation in a high-energy environment (rivers or channels, for example) often produces strong lateral changes in reflection characteristics, while slow deep sea sedimentation usually results in seismic facies that consist of a laterally continuous reflection pattern.

The first step in a seismic interpretation is the delineation and description of the different seismic facies units present. The rôle of seismic attributes in seismic stratigraphy is to aid in delineating seismic facies units and in quantifying seismic facies descriptions. For instance, reflection continuity can be quantified by measuring the degree of lateral change in reflectivity and IF.

Another application of seismic attribute analysis is the prediction of physical rock properties such as porosity or permeability from seismic data. Ground-truth is provided by measurement in a borehole. Lateral prediction away from the well is then obtained by correlating the physical parameter with the seismic attributes. In this application, the seismic attributes provide the input for a multivariate statistical analysis (using a neural network, for example).

In both the visual interpretation and the statistical pattern analysis applications, robust attribute extraction methods are of crucial importance. IF brings forward those characteristics from the image that in the standard image can be obscured by the large dynamic range in amplitude. Subtle changes in the spacing of reflectors are not neccesarily visible in the standard amplitude cross-section (see Figure 3(a), for example), but will be brought forward in an IF display.

IF estimates based on TFR peaks do not exhibit sufficient continuity in space to aid interpretation of the data. IF estimates based on the moments of the TFR provide a much more informative portrayal of the data [3], [19]. Figure 1 compares the IF estimates from three different TFRs on a seismic time signal. The fast hybrid IF estimate is very close to that obtained using the much more computationally expensive AOK TFR [3], [19]. The time resolution of the spectrogram IF estimate is significantly poorer than the other two methods. Moreover, a substantial smoothing is noticeable where rapid changes occur (at $t = 0.4$s, for example). Accurate localization in time of these rapid changes is important in seismic interpretation, as they may indicate important seismic facies sequence boundaries, which in turn may represent an important change in geological environment.

Figures 3(b) and 3(c) show complex-trace IF (8) and hybrid IF estimates (12) of the columns of the seismic section of Figure 3(a). To the left of the images, we plot the amplitude of the leftmost column. The wild fluctuations indicate that the complex-trace IF estimate is very noise-sensitive. The sharp peaks in the complex-trace IF estimate obscure the frequency trends of interest for a seismic facies analysis. Closely spaced seismic reflectors manifest themselves as bands of relatively high IF. The band of high-frequency reflections at $t = 0.4$s clearly stands out in the hybrid IF section, whereas it is difficult to localize in the amplitude display of Figure 3(a). Indeed, the abrupt change at $t = 0.4$s coincides with an important geological boundary. Lateral changes in reflector spacing and frequency are also more easily detected in the IF cross-section than in the amplitude data. For example, the reflection pattern below $t = 0.4$s exhibits less lateral continuity than the upper part of the section, indicating a different depositional environment.

Hybrid IF estimation is a computationally very efficient method for seismic attribute extraction. For visual interpretation, the hybrid IF provides a greatly enhanced image as compared to the complex-trace IF or the spectrogram average. The estimation algorithm potentiates the TFR-based interpretation of large seismic data volumes, which up to now has been severely inhibited by the large computational effort involved in calculating TFRs.

VI. Conclusions

We have presented a robust and efficient method for estimating time-frequency attributes of a signal. Using hybrid linear/quadratic time-frequency concepts avoids the expensive calculation of a quadratic or adaptive TFR. While we have focused on estimating the IF and instantaneous bandwidth, closed form expressions analogous to (9) can be developed for many other attributes, including higher-order time-frequency moments, kurtosis [4], and so on. Our results have particular relevance for seismic data analysis, where vast volumes of data require processing, and it is critical that efficient algorithms be used.

References

[1] B. Boashash, “Estimating and interpreting the instantaneous frequency of a signal, Part I: Fundamentals, Part II: Algorithms,” *Proc. IEEE*, vol. 80, no. 4, pp. 519–569, 1992.

[2] S. Haykin, R. Racine, Y. Xu, and C. Chapman, “Monitoring neuronal oscillations and signal transmissions between cortical regions using time-frequency analysis of electroencephalographic activity,” *Proc. IEEE*, vol. 84, no. 9, pp. 1295–1301, 1996.

[3] P. Steeghs and G. Drijkoningen, “Sequence analysis and attribute extraction with quadratic time-frequency representations.” submitted for publication, 2000.

[4] P. Loughlin and K. Davidson, “Instantaneous kurtosis,” *IEEE Signal Proc. Letters*, vol. 7, pp. 156–159, June 2000.

[5] B. Boashash and P. O’Sheah, “Use of cross Wigner-Ville distribution for estimation of instantaneous frequency,” *IEEE Trans. Signal Proc.*, vol. 41, pp. 1439–1445, Mar. 1993.

[6] F. Çakrak and P. Loughlin, “Instantaneous frequency estimation of polynomial phase signals,” in *Proc. IEEE Symp. Time-Freq. Time-Scale Anal.*, pp. 549–552, 1998.

[7] B. Ristic and B. Boashash, “Instantaneous frequency estimation of quadratic and cubic FM signals using the cross polynomial Wigner-Ville distribution,” *IEEE Trans. Signal Proc.*, vol. 44, pp. 1549–1553, 1993.

[8] S. Qian and J. Morris, “Wigner distribution decomposition and cross-terms deleted representation,” *Signal Processing*, vol. 27, pp. 125–144, May 1992.

[9] S. Qian and D. Chen, “Decomposition of the Wigner distribution and time-frequency distribution series,” *IEEE Trans. Signal Processing*, vol. 42, pp. 2836–2842, Oct. 1994.

[10] M. Pasquier, P. Gonçalvès, and R. Baraniuk, "Hybrid linear/bilinear time-scale analysis," *IEEE Trans. Signal Proc.*, vol. 47, pp. 254–259, Jan. 1999.

[11] D. Gabor, "Theory of communication," *J. IEE*, vol. 93, pp. 429–444, 1946.

[12] L. Cohen, *Time-Frequency Analysis.* Englewood Cliffs, N.J.: Prentice-Hall, 1995.

[13] D. Jones and R. Baraniuk, "An adaptive optimal-kernel time-frequency representation," *IEEE Trans. Signal Processing*, vol. 43, pp. 2361–2371, Oct. 1995.

[14] L. Cohen and C. Lee, "Instantaneous quantities, standard deviation and cross-terms," in *Proc. SPIE Conf. Adv. Alg. and Arch. for Signal Proc. III*, vol. 975, (San Diego (CA)), pp. 186–208, July 1988.

[15] P. Flandrin, *Time-frequency/Time-scale Analysis.* San Diego: Academic Press, 1999.

[16] O. Yilmaz, *Seismic Data Processing.* Tulsa, OK: Society of Exploration Geophysicists, 1987.

[17] T. Taner, F. Koehler, and R. Sheriff, "Complex seismic trace analysis," *Geophysics*, vol. 44, pp. 1041–1063, 1979.

[18] C. Payton, ed., *in AAPG Memoir*, ch. Seismic Stratigraphy — Applications to hydrocarbon exploration, pp. 301–328. Tulsa, OK: American Association of Petroleum Geologists, 1976.

[19] P. Steeghs and G. Drijkoningen, "Time-frequency analysis of seismic sequences," in *Proc. 65th SEG Meeting*, (Houston, TX), 1995.

List of Figures

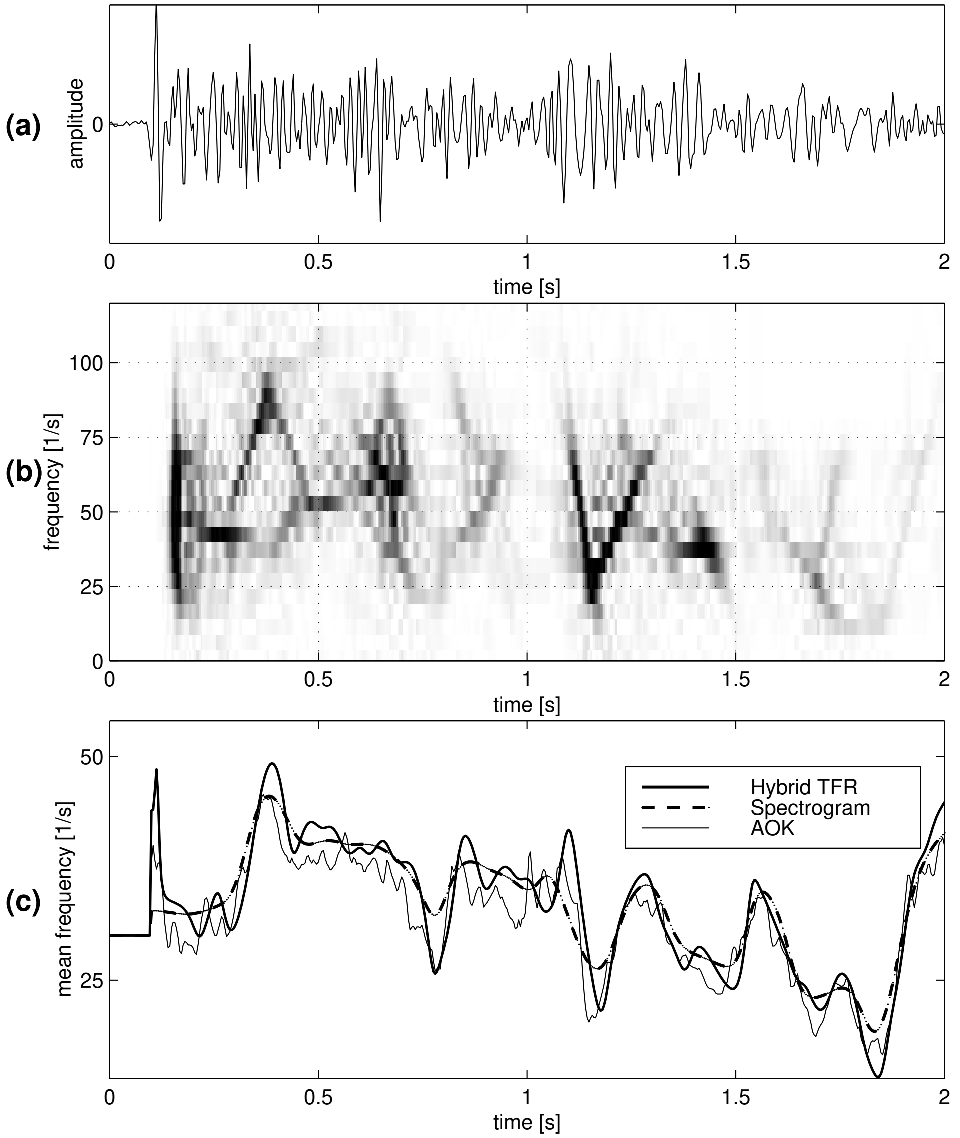

Fig. 1. Instantaneous frequency (IF) estimation of a seismic recording. (a) Seismic data, (b) adaptive time-frequency representation (TFR) [12] of the seismic trace, and (c) normalized instantaneous frequency estimates. Thick line is hybrid IF estimate (Manhattan distance threshold $\delta = 2$), dashed line adaptive TFR estimate, and thin line spectogram estimate. The hybrid IF estimate generated using no cross-terms (not shown) is very similar to the spectrogram estimate.

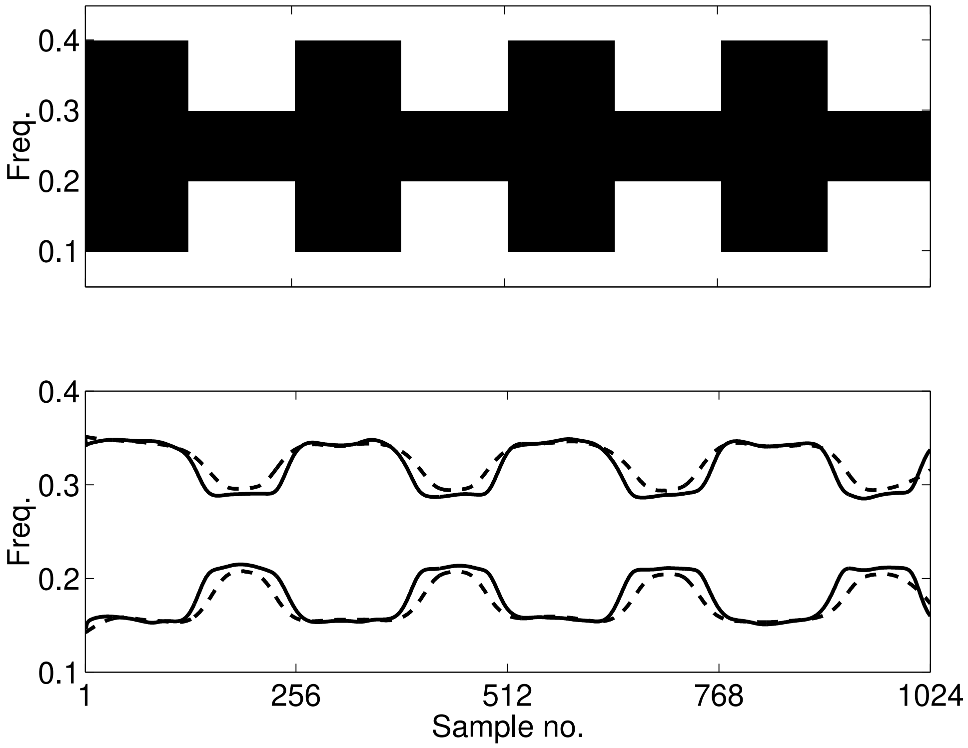

Fig. 2. Comparison between instantaneous bandwidth measures computed using the hybrid TFR approach and the spectrogram. White Gaussian noise was passed through a time-varying filter with (ideally) the frequency response in the top panel to generate 100 random realizations. The pass-band is indicated by the dark region. The lines in the bottom panel correspond to the averaged estimated IF ± the averaged estimated bandwidth $(v(t) \pm B(t))$ calculated using the hybrid approach with Manhattan distance threshold $\delta = 2$ (solid) and the spectrogram moments (dashed).

(a)

(b)

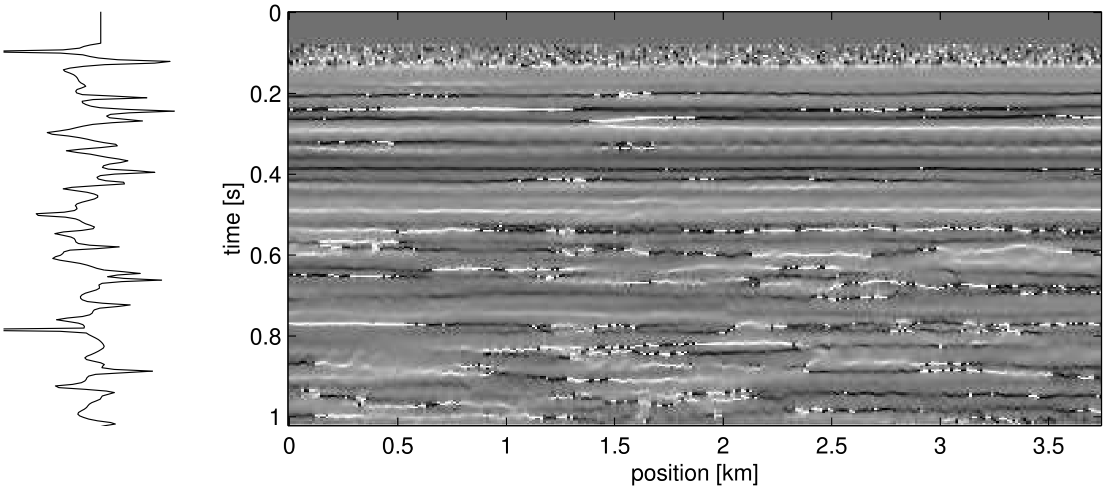
time [s]
0
0.2
0.4
0.6
0.8
1
position [km]
0
0.5
1
1.5
2
2.5
3
3.5

(c)

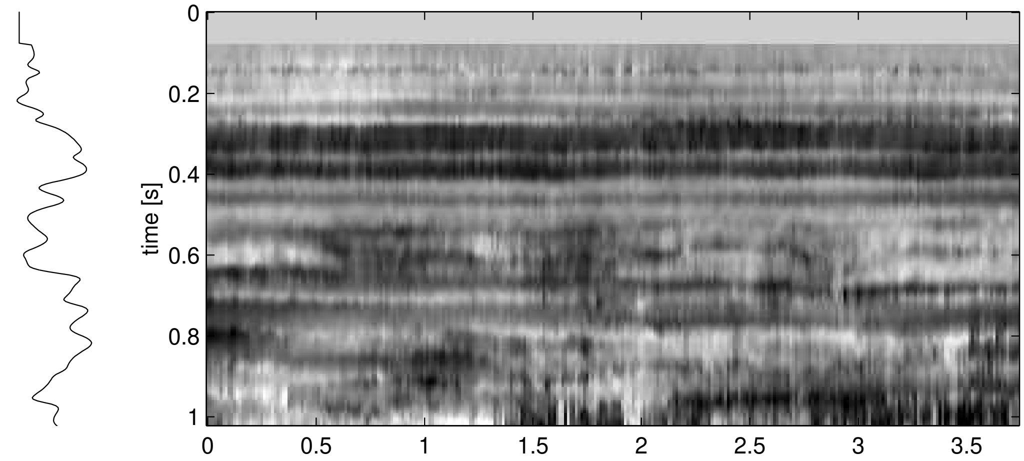
time [s]
0
0.2
0.4
0.6
0.8
1
position [km]
0
0.5
1
1.5
2
2.5
3
3.5